Int. J. Electrochem. Sci., 11 **(2016)** 1029 - 1040

International Journal of
ELECTROCHEMICAL
SCIENCE
www.electrochemsci.org

Effect of SO_4^{2-} and HCO_3^- to the Electrochemical Protection of FeS_{1-x} Scale to P110 Steel

Chengqiang Ren[1,2,], Jiameng Li, Wanguo Wang[1], Jingshi Hu[1], Li Liu[1], Junying Hu[2]*

[1] School of Materials Science and Engineering, Southwest Petroleum University, Chengdu, 610500, PR China
[2] State Key Laboratory of Oil and Gas Reservoir Geology and Exploitation, Southwest Petroleum University, Chengdu, 610500, PR China
[*]E-mail: chengqiangren@163.com

Received: 21 October 2015 / *Accepted:* 19 November 2015 / *Published:* 1 January 2016

The electrochemical protection of FeS_{1-x} scale to the P110 steel in two different solutions were researched by designed experiments including Mott-Schotty, potentiodynamic polarization, electrochemical impedance spectroscopy and weight loss. To understand some aspects of the mechanism, XRD, XPS and SEM were also adapted. FeS_{1-x} scale in 0.5 mol/L Na_2SO_4 solution presented lower protection to the steel, because the electron transfer and mass diffusion in the scale were easy. After immersion, the Fe/S atomic ratio of scale decreased, which resulted in increasing cation vacancy. As a result, p-type semiconducting property was found. However, the electron transfer and mass diffusion in the scale were mitigated in $NaHCO_3$ solution, so the electrochemical protection to the steel was enhanced. On the contrary, the Fe/S atomic ratio of scale changed little. High anodic polarization resistance inhibited diffusion of Fe^{2+}. Fe^{2+} became interstitial cation by this way. The n-type semiconducting property, thus, was observed.

Keywords: Electrochemical protection; Electron transfer; Mass diffusion; P 110 steel

1. INTRODUCTION

Steels in oil and gas industry face severe challenge of H_2S corrosion in H_2S-containning environments, because the sulfate-reduction results in dissolution of Fe [1]. The sulfide film deposits on the surface of steel by the subsequent electrochemical reaction between the anodic and cathodic primary products, which determines the corrosion rate of steel [2,3].

After studying the corrosion scale, many phases in the Fe-S system, including mackinawite, cubic ferrous sulfide, pyrrohtite, troilite and pyrite, were measured under different conditions [4-6].

Thus, two types of non-stoichiometric ferrous sulfides are always classified in various aggressive environments based on the total atom ratio of Fe/S. When x is limited in the range of 0 to 1, FeS_{1+x} represents S rich scale, and Fe rich scale is expressed as FeS_{1-x}.

It is worth investigating and analyzing the property of the sulfide corrosion scale, because it can strongly influence the corrosion kinetics. This work mainly focuses on the electrochemical protection of FeS_{1-x} scale. We should pay more attentions to SO_4^{2-} and HCO_3^- because too much works have been aimed on corrosion in petroleum industry in Cl^- containing solution [7-9]. There lack essential data on the role of SO_4^{2-} and HCO_3^- to corrosion in H_2S-containing environments.

Corrosion in electrolyte is an electrochemical reaction process. The rate is determined by electron transfer and mass diffusion, especially in the corrosion scale. Thus, the FeS_{1-x} scale was prepared on P110 steel by corrosion experiment in H_2S dissolved purified water. The conductivity of the scale was evaluated by semiconducting property when Mott-Schotty curves were measured, and the mass diffusion was determined by EIS and potentiodynamic polarization. The weight loss method was adapted to prove the electrochemical prediction. The composition and microstructure is in favor of assumption to mechanism.

2. EXPERIMENTAL

2.1 Material pretreatment

P110 steel, with chemical compositions of C 0.26, Si 0.25, Mn 1.71, Ni 0.02, Cr 0.05, Mo 0.01, Ti 0.01 and Fe balance in weight percent (wt%), was cut to 50×10×2 mm rectangular plate. The surface of steel was polished with sub micron alumina pastes, and then it was degreased with acetone, washed in distilled water, rinsed with alcohol and dried.

2.2 Sample preparation

FeS_{1-x} scale was prepared under carefully controlled oxygen-free but H_2S-containing conditions. The steels were hanged in distilled water in an autoclave. After adequately deaerated by N_2 gas, 1 MPa H_2S was injected into the autoclave. Corrosion scale was formed on the surface of P110 steel at 308K after 72 h. Subsequent 72 h immersion of the scale covered steels were respectively operated in 0.5 mol/L Na_2SO_4 solution and 0.5 mol/L $NaHCO_3$ solution.

2.3 Characterization measurement

XRD of the scale was measured by the DX-2000 X-ray diffractometer with a Cu Kα radiation. The composition of the sample was analyzed by X-ray photoelectron spectrometer using a XSAM800 apparatus and the data were identified with the XPSPEAK41 software.

The microstructure of scale was observed by SEM on a JSM-6490LV scanning electron microscope.

Capacitance measurement to the scale was carried out using HEWLETT PACKARD 4P4384A model inductance-capacitance-resistance meter to obtain the dielectric constant.

The scale sample was used as the working electrode in a three electrode cell with a platinum plate counter electrode and a saturated calomel reference electrode (SCE). The Autolab Model PGSTAT302N electrochemical potentiostat was used to carry out electrochemical measurements. During Mott-Schottky measurement, the frequency was fixed at 1 kHz, and the potential scanning rate was 50 mV s^{-1}. The potentiodynamic polarization was operated by a scan rate of 0.5 mV s^{-1}. EIS was measured from 10 kHz to 10 mHz by AC amplitude of 10mV at open potential.

Corrosion rate of P110 steel was calculated by the method of weight loss after exposure in designed conditions. Six specimens in each case were used to obtain the average value. The corrosion rate, v (mm/a), is defined thickness reduction of steel per year.

3. RESULTS AND DISCUSSION

3.1. FeS_{1-x} scale

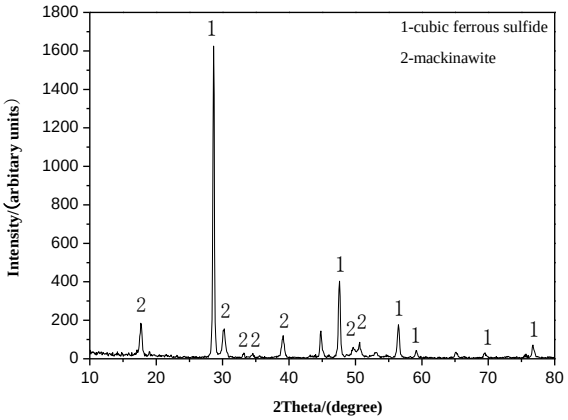

Figure 1. XRD Pattern of the prepared scale in H_2S dissolved water

The XRD pattern in Figure 1 shows the main phases in the corrosion scale are cubic ferrous sulfide and mackinawite. The mackinawite was judged from the characteristic peaks at phase angle (2θ) values of 17.68°, 30.09°, 38.99° and 50.45° corresponding to lattice planes (0 0 1), (1 0 1) , (1 1 1) and (1 1 2), respectively, with a lattice constant of a=b=3.674Å and c=5.033Å. The product is attributed to the adsorption of HS^- to the surface of bare steel and the following electrochemical reactions at the initial period. The most suggestion to the overall reaction is given by equation (1) [10-11].

$$Fe + HS^- \rightarrow FeS_{1-x} + xSH^- + (1-x)H^+ + 2e^- \quad (1)$$

In harmony with this, the testimony of cubic ferrous sulfide is the characteristic peaks at phase angle (2θ) values of 28.49°, 47.46° and 56.26° corresponding to lattice planes (1 1 1), (2 2 0) and (3 1

1), respectively, with a lattice constant of a = 5.419Å. The cubic FeS was first identified by de Medicis [12]. It cannot be found naturally but forms as a product by the electrochemical corrosion reaction in H_2S-containing medium [13]. The appearance of cubic ferrous sulfide was regarded as the further product of mackinawite. The phase transformation was observed by epitaxial growth at the interface between the tetragonal iron sulfide and the hydrogen sulfide solution.

S^{2-} accelerates the formation of FeS based on the cathodic reaction at scale/solution interface:

$$2HS^- + 2e^- \rightarrow S^{2-} + H_2 \quad (2)$$

$$FeS_{1-x} + xS \rightarrow FeS \quad (3)$$

We only focus on concentrations of iron ion and sulfur ion in the scale to obtain the ratio of Fe/S in non-stoichiometric ferrous sulfides by S(2p) and Fe(2p) XPS spectra. Iron atom and sulfate radical were neglected in the discussion. The XPS spectrum of the original scale before immersion test is pictured in Figure 2.

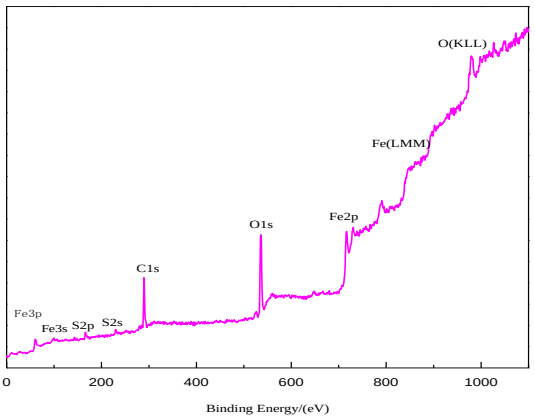

(a) Wide spectrum

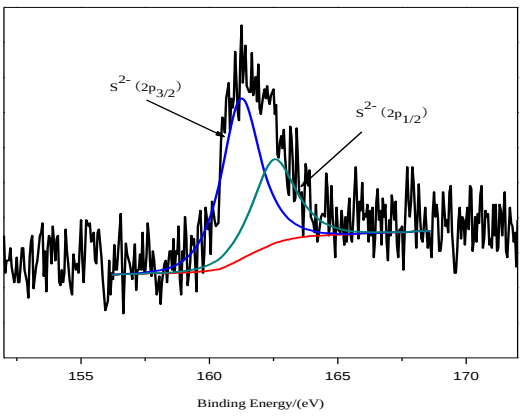

(b) S 2p spectrum

Figure 2. XPS spectrum of the original scale prepared in H_2S dissolved water

Binding energies for sulfur and corresponding analyses are listed in Table 1. The binding energy shifts were fitted using doublets ($2p_{3/2}$, $2p_{1/2}$) for S^{2-} [14-19]. Peaks at 161.2 eV and 162.5 eV of sulfur mean existence of S^{2-} but without SO_4^{2-}. It is calculated that the ratio of Fe/S was 1.95.

Table 1. XPS Parameters for S 2p Spectra in different scales

Samples	Binding Energy(eV)	FWHM(eV)	Species*
Original scale	161.2	1.782	S^{2-} ($2p_{3/2}$) [14]
	162.5	1.956	S^{2-} ($2p_{1/2}$) [15]
Scale in Na_2SO_4	161.2	1.899	S^{2-} ($2p_{3/2}$) [14]
	162.7	2.288	$(S\text{-}S)^{2-}$ ($2p_{3/2}$) [17-19]
	168.3	2.880	SO_4^{2-}($2p_{3/2}$) [16]
Scale in $NaHCO_3$	161.2	1.776	S^{2-} ($2p_{3/2}$) [14]
	162.5	1.972	S^{2-} ($2p_{1/2}$) [15]

*Note: The cited references reported corresponding species at the same binding energy.

3.2. Electron transfer

The charge distribution at the semiconductor/electrolyte interface is always determined by measuring the capacitance of the space-charge layer (C_{sc}) as a function of the electrode potential (E). C_{sc} at different applied E can be expressed as [20, 21]:

$$\frac{1}{C_{SC}^2} = \frac{2}{\varepsilon_0 \varepsilon N_D A^2}\left(E - E_{FB} - \frac{kT}{e}\right) \quad \text{for n-type semiconductor} \tag{4}$$

$$\frac{1}{C_{SC}^2} = -\frac{2}{\varepsilon_0 \varepsilon N_A A^2}\left(E - E_{FB} - \frac{kT}{e}\right) \quad \text{for p-type semiconductor} \tag{5}$$

Where ε_r is the relative dielectric constant of the specimen, ε_0 is the permittivity of free space (8.854×10^{-14} F cm^{-1}), e is the electron charge(1.602×10^{-19} C), A is the sample area (cm^2), N_D and N_A are the donor density (cm^{-3}) and acceptor density (cm^{-3}), E_{FB} is the flat band potential (V), k is the Boltzmann constant (1.38×10^{-23} J K^{-1}), and T is the absolute temperature (K). From the plot of C_{sc}^{-2} versus E, the values of N_D, N_A and E_{FB} can be calculated.

Figure 3 shows the Mott-Schottky plots for two samples after immersed in Na_2SO_4 solution and $NaHCO_3$ solution, respectively. The existence of a negative linear relationship between C^{-2} and E in Na_2SO_4 solution in the potential range from -0.5 V to 0.5 V indicates p-type semi-conductive property. On the contrary, the positive slope in the potential range from 0V to 0.75 V means n-type semi-conductive property is found in $NaHCO_3$ solution.

In order to obtain the semiconducting parameters, evaluation of dielectric properties of FeS_{1-x} scale is necessary. It was calculated by equation (6).

$$\varepsilon_r = \frac{C_p}{C_0} = \frac{tC_p}{\varepsilon_0 S} \quad (6)$$

where C_p, C_0, ε_0, S and t are capacitance of the sample, capacitance of vacuum, the constant of permittivity for free space, the cross-sectional area of the flat surface and thickness of FeS_{1-x} wafer, respectively.

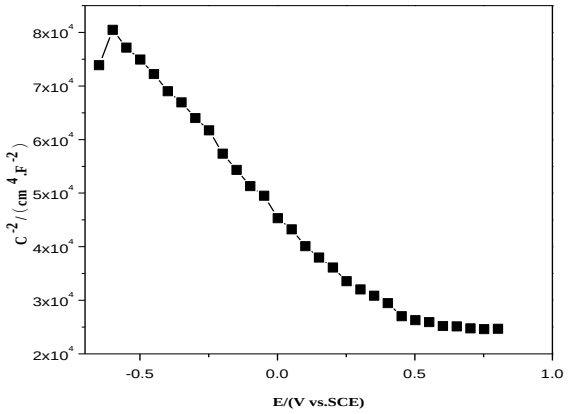

(a) Na_2SO_4 solution

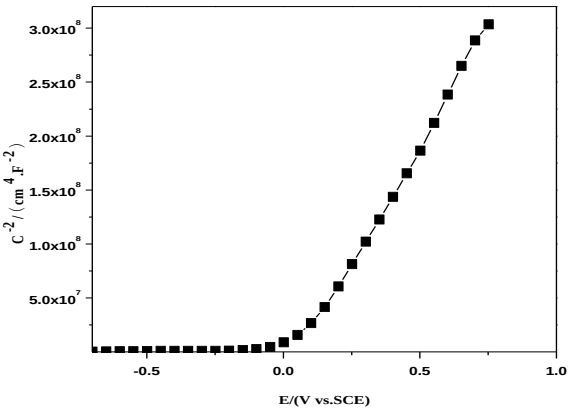

(b) $NaHCO_3$ solution

Figure 3. Mott-Schottky plots of FeS_{1-x} scale after exposure in different electrolytes

The dielectric constant value in equations (4) and (5) is 500 corresponding to 1 kHz which is the frequency given during Mott-Schottky measurement. It is calculated by the value tested by HEWLETT PACKARD 4P4384A model inductance-capacitance-resistance meter.

By fitting the linear segment, N_A in Na_2SO_4 solution is 5.25×10^{20} cm^{-3}, but N_D in $NaHCO_3$ solution is 6.29×10^{17} cm^{-3}. The acceptor density of the sample in Na_2SO_4 solution is much higher than the donor density of the sample in $NaHCO_3$ solution. The higher acceptor density or donor density

results in higher electroconductivity of the scale, which accelerates the corrosion process from dynamics analysis because the electron takes part in the electrochemical reaction.

According to semiconductive theory, the electron transfer in n-type semiconductor is dominated by interstitial cation or anion vacancy, and cation vacancy determines the electron transfer in p-type semiconductor. In the scale, the doped interstitial cation is only Fe^{2+}, so the Fe/S in $NaHCO_3$ solution should be higher than it in Na_2SO_4 solution.

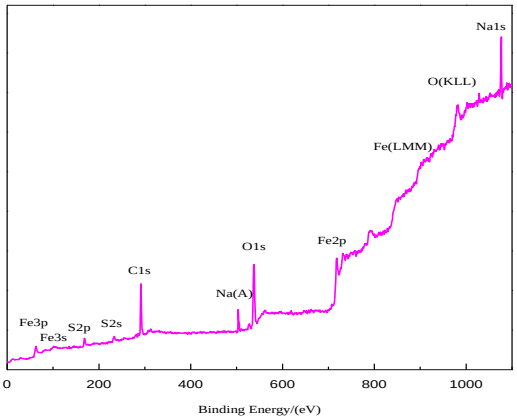

(a) Wide spectrum

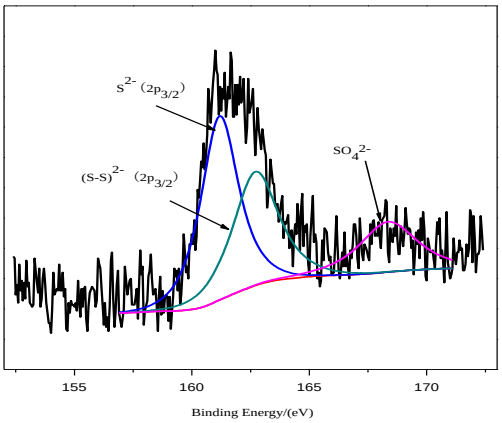

(d) S 2p spectrum

Figure 4. XPS spectrum of the scale after immersion in Na_2SO_4 solution

Figure 4 shows the XPS spectrum of the scale after immersion in Na_2SO_4 solution. The ratio of Fe/S changes to 1.18. The S(2p) spectra contain two principal peaks at 161.2 eV and 162.7 eV. References showed that the most intense peak at 162.7 eV represented the contribution of S atoms of S-S dimmers residing on bulk sites of FeS_2. SO_4^{2-} has adsorption capacity to solid iron compound, such as FeS_{1-x} and FeS. To maintain electroneutrality, the FeS_{1-x} and FeS also adsorb H^+ [22]. The dissolution of scale leads to Fe^{2+} losing and Fe/S increasing.

$$FeS_{1-x} + (1-x)H^+ \rightarrow Fe^{2+} + (1-x)HS^- + 2xe \quad (7)$$

$$FeS_{1-x} + 2xHS^- \rightarrow FeS_{1+x} + 2xH^+ + 4xe^- \quad (8)$$

$$2FeS + 2HS^- \rightarrow 2FeS_2 + H_2 + 2e^- \quad (9)$$

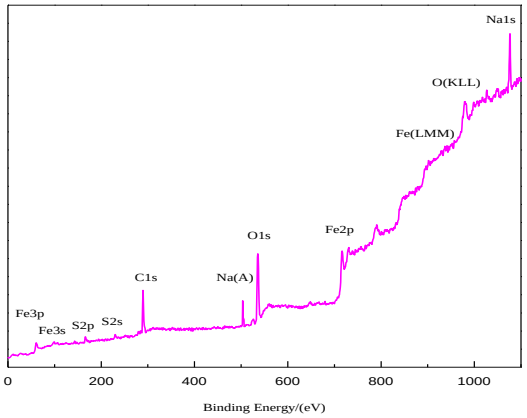

(a) Wide spectrum

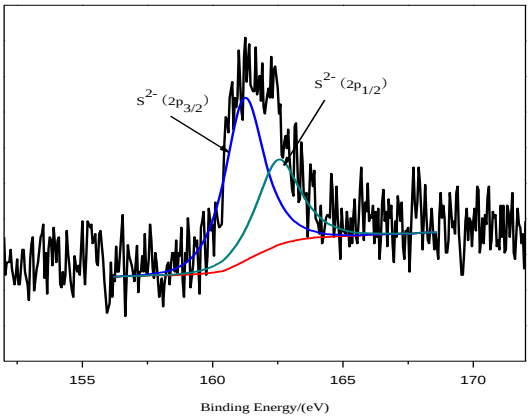

(b) S 2p spectrum

Figure 5. XPS spectrum of the scale after immersion in $NaHCO_3$ solution

Figure 5 show the XPS spectra for the scale after immersed in $NaHCO_3$ solution. It is similar to the original scale. S^{2-} in polysulfides is determined at 161.2 eV and 162.5 eV. At the same time, the ratio of Fe/S, 1.90, changes little.

3.3. Mass diffusion

The potentiodynamic polarization curves of the samples after immersed in Na_2SO_4 solution and $NaHCO_3$ solution are shown in Figure 6. It can be observed passivation in the wide potential range of -0.8 to 0.7 V in $NaHCO_3$ solution, while activation polarization is found in Na_2SO_4 solution. Tafel

slopes were fitted by the data in strong polarization zone. In Na_2SO_4 solution, b_a=107 mV/d and b_k=127 mV/d mean that the cathodic reaction rate is close to the anodic one. Though the cathodic Tafel slope (b_k=162 mV/d) in $NaHCO_3$ solution increases slightly, the scale plays more important role on the anodic process, because the passivation greatly mitigates the reaction rate.

Figure 7(a) shows the Nyquist plot of EIS. To describe the equivalent circuits shown in Figure 7(b) and 7(c), the measured data were fitted. The parameters include solution resistance (R_s), reaction resistance (R_t), double layer capacitance (Q_{dl}) and Warburg resistance (Z_w).

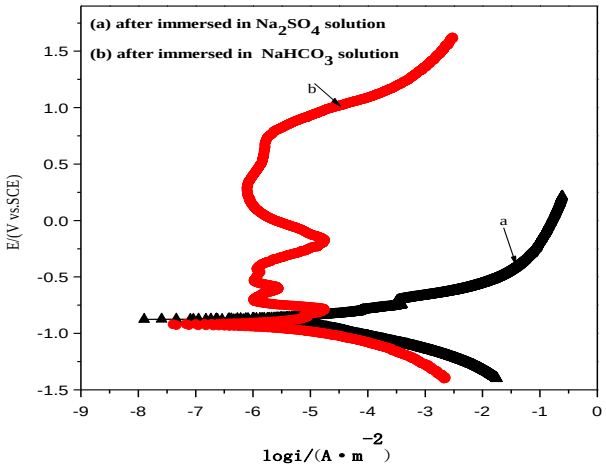

Figure 6. Polarization curves of the samples after exposure in different solutions

A simple capacitive loop can well fit the profile in Na_2SO_4 solution, but a Warburg resistance is suggested to add to the capacitive loop in $NaHCO_3$ solution. Warburg resistance is always caused by mass (reactants or products) diffusion in the scale [23, 24]. It means the mass diffusion controls the corrosion development in $NaHCO_3$ solution.

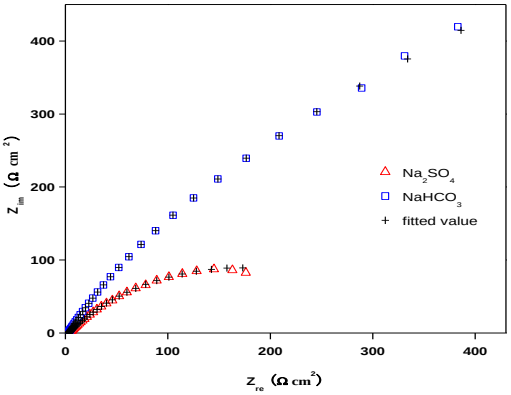

(a) Nyquist plot

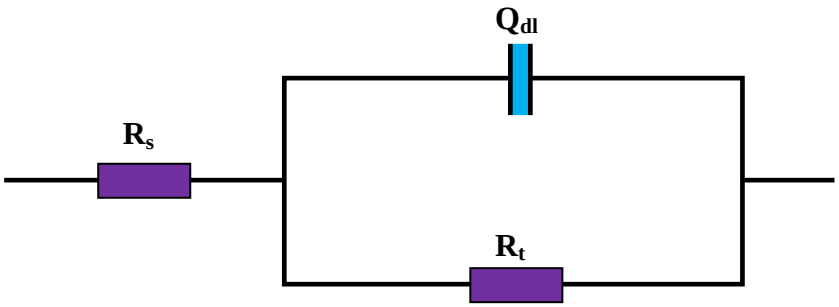

(b) Equivalent circuit for sample in Na_2SO_4 solution

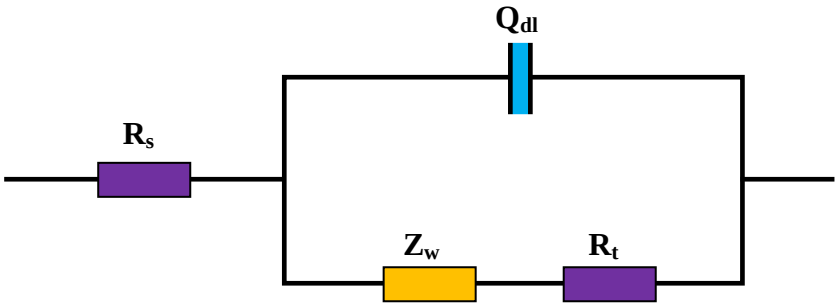

(c) Equivalent circuit for sample in $NaHCO_3$ solution

Figure 7. EIS and equivalent circuits of the samples after exposure in different solutions

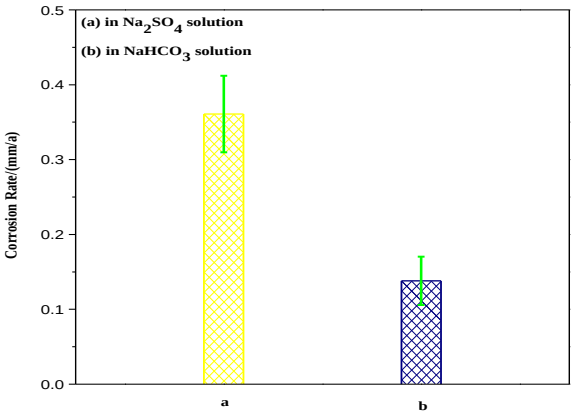

Figure 8. Corrosion rates of samples after immersion in different solutions

It has been pointed that the doping of cation interstitial or anion vacancy in the scale plays role of inhibiting cations from metal underneath the covered layer [25]. That is to say, the scale inhibits the Fe^{2+} transferring from the steel/scale interface to the scale/electrolyte interface. Just because of this, Fe^{2+} dopes in scale as an interstitial cation, which presents a n-type semiconducting property.

3.4. Corrosion resistance

The corrosion rate was calculated by equation (10):

$$v = \frac{8.76\Delta m}{st\rho} \quad (10)$$

where, Δm (g) is the weight loss of the sample after corrosion, s (m^2) is the exposed surface area, t (h) is the corrosion time, and ρ (g cm^{-3}) is the density of steel. The results of P110 steel samples after exposure in different conditions is pictured in Figure 8. The corrosion rate in Na_2SO_4 solution is much higher than that in $NaHCO_3$ solution.

Figure 9 shows the surface morphology of the scale after immersed in solution. The integrity of out-layer scale was damaged by the role of Na_2SO_4. To the contrary, many white products deposited on the surface to densify the scale in $NaHCO_3$ solution. The later feature is favorable to protection of scale to the steel.

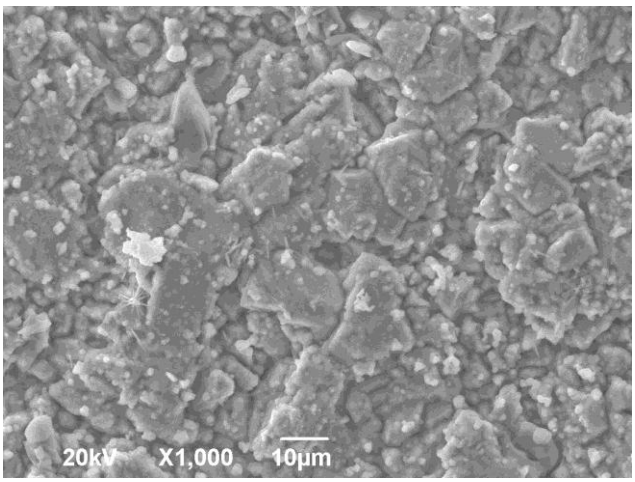

(a) Na_2SO_4 solution

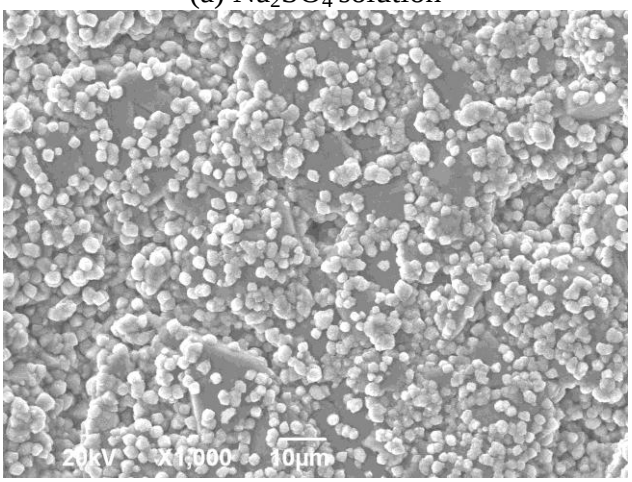

(b) $NaHCO_3$ solution

Figure 9. Surface morphology of FeS_{1-x} scale after immersion in different electrolytes

4. CONCLUSIONS

The FeS_{1-x} scale was prepared by using P110 steel in H_2S dissolved water. The effect of SO_4^{2-} and HCO_3^- to the electrochemical protection of FeS_{1-x} scale to P110 steel was investigated in Na_2SO_4 and $NaHCO_3$ solutions.

(1) FeS_{1-x} scale in $NaHCO_3$ solution presents n-type semiconducting property with lower electron conductivity and slower mass diffusion, which ensures good protection to the steel.

(2) FeS_{1-x} scale in Na_2SO_4 solution presents p-type semiconducting property with higher electron conductivity and faster mass diffusion, which decreases the protective ability.

ACKNOWLEDGEMENTS
This research was sponsored by the National Natural Science Foundation of China (51374180) and the Education Office Fund of Sichuan Province (14CZ0006).

References

1. W. Sun and S. Nešić, *Corrosion/07*, NACE, 2007, Paper No. 655.
2. Z. Q. Bai, Z. F. Yin, D. Wei, X. F. Wang and C. X. Yin, *Mater. Corros.*, 61 (2010) 389.
3. B. Brown and S. Nešić, *Corrosion/05*, NACE, 2005, Paper No. 625.
4. P. Bai, S. Zheng, H. Zhao, Y. Ding, J. Wu and C. Chen, *Corr. Sci.*, 87 (2014) 397.
5. J. Tanga, Y. Shaoa, J. Guoc, T. Zhanga, G. Menga and F. Wanga, *Corros. Sci.*, 52 (2010) 2050.
6. A. Hernández-Espejel, M. A. Domínguez-Crespo, R. Cabrera-Sierra, C. Rodríguez-Meneses and E. M. Arce-Estrada, *Corros. Sci.*, 52 (2010) 2258.
7. X. Xu, J. Miao, Z. Bai, Y. Feng, Q. Ma and W. Zhao, *Appl. Surf. Sci.*, 258 (2012) 8802.
8. Z. Qiu, C. Xiong, Z. Chang, Z. Zhao, C. Zhao and Z. Ye, *Petrol. Explor. Dev.*, 39 (2012) 256.
9. Y. Choi, S. Nešić and S. Ling, *Electrochim. Acta*., 56 (2011) 1752.
10. J. G. Deng, W. Yan, X. R. Li and X. G. Deng, *Petrol. Sci. Technol.*, 29 (2011) 1387.
11. C. Q. Ren, X. Wang, L. Liu, H. E. Yang and N. Xian, *Mater. Corros.*, 63 (2012) 168.
12. R. de Médicis, *Science*. 170 (1970) 191.
13. M. A. Lucio-Garcia, J. G. Gonzalez-Rodriguez, M. Casales, L. Martinez, J. G. Chacon-Nava, M. A. Neri-Flores and A. Martinez-Villafañe, *Corros. Sci.*, 51 (2009) 2380.
14. D. S. Han, B. Batchelor and A. Abdel-Wahab, *Environ. Prog. Sustain.*, 32 (2013) 84.
15. G. Pratesi and C. Cipriani, *Eur. J. Mineral.*, 12 (2000) 397.
16. M. El Azhar, M. Traisnel, B. Mernari, L. Gengembre, F. Bentiss and M. Lagrenee, *Appl. Surf. Sci.*, 185 (2002) 197.
17. H. W. Nesbitt, M. Scaini, H. Höchst, G. M. Bancroft, A. G. Schaufuss and R. Szargan, *Am. Mineral.*, 85 (2000) 850.
18. B. C. Bostick and S. Fendorf, *Geochim. Cosmochim. Acta*., 67 (2003) 909.
19. Y. F. Cai, Y. G. Pan, J. Y. Xue, Q. F. Sun, G. Z. Su and X. Li, *Appl. Surf. Sci*,. 225 (2009) 8750.
20. I. M. Gadala and A. Alfantazi, *Appl. Surf. Sci.* 357 (2015) 356.
21. M. Lashgari., N. Shafizadeh and P. Zeinalkhani, *Sol. Energ. Mat. Sol. C*., 137 (2015) 274.
22. A. G. Wikjord, T. E. Rummery, F. E. Doern and D. G. Owen, *Corros. Sci.*, 20 (1980) 651.
23. P. Bai, S. Zheng and C. Chen, *Mater. Chem. Phys.*, 149-150 (2015) 295.
24. S. Skale, V. Doleček and M. Slemnik, *Prog. Org. Coat*., 62 (2008) 387.
25. M. C. L. de Oliveira, V. S. M. Pereira, O. V. Correa, N. B. de Lima and R. A. Antunes, *Corros. Sci.*, 69 (2013) 311.